Characteristic dark matter density profiles in a strictly MDAR-following Universe

Virinchi V. Rallabhandi [*]

University of Western Australia, 35 Stirling Highway, Crawley, 6009, Australia

ABSTRACT

A fundamental tenet of MOdified Newtonian Dynamics (MOND) is the Mass Discrepancy Acceleration Relation (MDAR) - a direct link between the acceleration observed and that predicted from Newton's laws with a significant disparity only when the acceleration is lower than a MOND acceleration constant, $g_\dagger$. Recent observations suggest MDAR indeed holds - at least statistically - on galaxy scales. Here, I consider the implications for dark matter assuming its distribution is such that MDAR is strictly reproduced. I examined the best power law approximation to the dark matter density profile, $\frac{\mathrm{d}\ln\rho_{\mathrm{DM}}}{\mathrm{d}\ln r}$, across various prescriptions for MOND interpolating function and baryonic mass distribution; there were very few cases in which the results agreed with those from ΛCDM simulations. Hence, I see a distinguishing feature between MOND and ΛCDM. While MDAR must hold strictly in MOND, it can only ever hold qualitatively in ΛCDM.

Key words: dark matter – acceleration of particles – galaxies: kinematics and dynamics

1 INTRODUCTION

One of the biggest conundrums of our generation is the nature of "dark-sector" physics. Like many enduring debates in the history of science, it has polarised opinion while eluding solution. Dark matter is fascinating in particular; despite almost 40 years of work, we have yet to detect any dark matter nor truly discredit its rival, MOdified Newtonian Dynamics (MOND). The flame has most recently been rekindled by McGaugh, Lelli & Schombert (2016) - hereafter MLS16. They showed the radial acceleration due to a galaxy's[1] baryons[2], g_{bar}, is strongly correlated with the radial acceleration observed, g_{obs}, by

$$g_{\mathrm{obs}} = \frac{g_{\mathrm{bar}}}{1 - e^{-\sqrt{g_{\mathrm{bar}}/g_\dagger}}} \tag{1}$$

where $g_\dagger = 1.2 \times 10^{-10}\, m/s^2$. As Mordehai Milgrom - MOND's inventor - was quick to point out (Milgrom 2016), equation (1) is an example of the Mass Discrepancy Acceleration Relation (MDAR) - a fundamental MOND prediction whose form has been updated regularly (see Sanders 1990; Gentile, Famaey & de Blok 2011, for some previous iterations). MDAR is an incredibly powerful statement. One can fully determine a galaxy's dynamics from its visible matter alone; no assumptions about dark matter's existence or form are necessary.

However, it's still useful at times to adopt a dark matter point of view because whether you believe in dark matter or not, a missing mass component - the mass discrepancy - can always be added to explain the visible dynamics. Dark matter is analogous to a pseudo-force when applying Newton's laws in non-inertial reference frames. The force isn't really there, but it's often an efficient way to predict the equations of motion. Since

$$g_{\mathrm{obs}} = g_{\mathrm{bar}} + g_{\mathrm{DM}} \iff g_{\mathrm{DM}} = g_{\mathrm{obs}} - g_{\mathrm{bar}} \tag{2}$$

---

[*] E-mail: rvirinchi@gmail.com

[1] Throughout this paper, when I say "galaxy," I'm really only referring to rotationally supported galaxies.

[2] For consistency with the field's literature, I take "baryons" to mean all normal matter, even though electrons and the like are not baryons.

equation (1) can be re-written as

$$g_{\mathrm{DM}} = \frac{g_{\mathrm{bar}}}{\mathrm{e}^{\sqrt{g_{\mathrm{bar}}/g_\dagger}} - 1} \tag{3}$$

MLS16 only made passing reference to this formulation of MDAR, but it's quite profound in its own right because g_{DM} is enough to calculate ρ_{DM}, the volume mass density distribution of dark matter; I'll leave the calculation's details to the equation overload of section 2. Therefore, regardless of whether dark matter exists, one can deduce the theoretical distribution required to reproduce the observed dynamics given Newtonian gravity.

Across sections 2 and 3, I deduce ρ_{DM} for various prescriptions of ρ_{bar} and MOND interpolating functions consistent with MLS16's data. In all cases, the ρ_{DM} profile is inconsistent with the ever popular isothermal sphere, cored isothermal sphere, NFW (Navarro, Frenk & White 1997), Burkert (Burkert 1995) or more recent DC14 (Di Cintio et. al 2014) profiles. Di Cintio et. al's profile is especially notable for it tries to account for baryons' effect on ρ_{DM} - an aspect regularly ignored by works of previous generations.

In summary, the ρ_{DM} profiles required to strictly reproduce MDAR are unlike those required by dark matter simulations. The discord is especially important in light of global efforts to reproduce MLS16's result under the ΛCDM paradigm (see Navarro et al. 2017; Ludlow et al. 2017; Keller & Wadsley 2017, for some examples). My result shows it is impossible for such simulations to reproduce MDAR exactly while remaining consistent with earlier work; the best they can do is approximate it across a galaxy. Therefore, we have a fundamental disparity between MOND and ΛCDM. While MDAR is followed strictly throughout a galaxy in MOND, it cannot be in ΛCDM. Indeed, it need not be for ΛCDM to be true. MLS16's presentation of the data doesn't help discriminate between the two paradigms. They only present beautifully averaged, binned data. Instead, with measurements revealing how strictly MDAR is followed within each galaxy, we may finally be able to settle the enduring feud between MOND and dark matter.

Before I dive into details, I'd like to acknowledge this paper does not present entirely new ideas. Rather, it is an offshoot of work I began in Rallabhandi & Meurer (2019) - hereafter RM19. For clarity and completeness I will repeat some of the material in section 6 of that work. Overall, I believe I'm presenting a more refined, focused and holistic approach here.

2   MATHEMATICAL MACHINERY

2.1   Deriving the dark matter distribution

I want to determine the implied dark matter distribution under the assumption MDAR holds strictly. I'm going to assume the only significant force at play in the galaxy is gravity and the dark matter interacts gravitationally with all massive objects (including itself). For those who do not wish to re-live the torture inflicted upon them by school teachers trying to imprint the chain, product and quotient rules on their minds, the salient results are equations (18), (24), (27) and (28) along with the general discussions in sections 2.2 and 2.3.

$$\therefore g_{\mathrm{obs}} = g_{\mathrm{bar}} f(g_{\mathrm{bar}}/g_\dagger) \tag{4}$$

where $g_\dagger$ is the MOND acceleration constant and f is an arbitrary MOND interpolating function, i.e. $f(x) \approx 1$ for $x \gg 1$ and $f(x) \approx \frac{1}{\sqrt{x}}$ for $x \ll 1$.

$$\therefore g_{\mathrm{DM}} = g_{\mathrm{obs}} - g_{\mathrm{bar}} \tag{5}$$
$$= g_{\mathrm{bar}}(f(g_{\mathrm{bar}}/g_\dagger) - 1) \tag{6}$$

I'm focussing solely on the case where ρ_{DM} is spherically symmetric. Hence, g_{DM} and Φ_{DM}, the gravitational potential due to the dark matter alone, are also spherically symmetric.

$$\therefore g_{\mathrm{DM}} = \frac{\mathrm{d}\Phi_{\mathrm{DM}}}{\mathrm{d}r} \tag{7}$$

Strictly speaking, $g_{\mathrm{DM}} = -\frac{d\Phi_{\mathrm{DM}}}{dr}$, but that expression uses $g_{\mathrm{DM}} < 0$ for rotationally supported systems. However, if we relabel $g_{\mathrm{DM}} > 0$, i.e. take the radial acceleration to be positive in the $-r$ direction, then we get equation (7). Hence, we can bypass the annoying clutter and confusion of minus signs in the subsequent discussion. For Newtonian gravity, we can apply Poisson's

equation,

$$4\pi G\rho_{\text{DM}} = \nabla^2\Phi_{\text{DM}} \tag{8}$$

$$= \frac{1}{r}\frac{\text{d}^2}{\text{d}r^2}\left(r\Phi_{\text{DM}}\right) \tag{9}$$

$$= \frac{1}{r}\frac{\text{d}}{\text{d}r}\left(\frac{\text{d}}{\text{d}r}\left(r\Phi_{\text{DM}}\right)\right) \tag{10}$$

$$= \frac{1}{r}\frac{\text{d}}{\text{d}r}\left(\Phi_{\text{DM}} + r\frac{\text{d}\Phi_{\text{DM}}}{\text{d}r}\right) \tag{11}$$

$$= \frac{1}{r}\frac{\text{d}}{\text{d}r}\left(\Phi_{\text{DM}} + rg_{\text{DM}}\right) \tag{12}$$

$$= \frac{1}{r}\left(g_{\text{DM}} + g_{\text{DM}} + r\frac{\text{d}g_{\text{DM}}}{\text{d}r}\right) \tag{13}$$

$$= \frac{2g_{\text{DM}}}{r} + \frac{\text{d}g_{\text{DM}}}{\text{d}r} \tag{14}$$

Then, using equation (6),

$$4\pi G\rho_{\text{DM}} = \frac{2g_{\text{bar}}(f(\frac{g_{\text{bar}}}{g_\dagger}) - 1)}{r} + \frac{\text{d}}{\text{d}r}\left(g_{\text{bar}}\left(f\left(\frac{g_{\text{bar}}}{g_\dagger}\right) - 1\right)\right) \tag{15}$$

$$= \frac{2g_{\text{bar}}(f(\frac{g_{\text{bar}}}{g_\dagger}) - 1)}{r} + \frac{\text{d}}{\text{d}g_{\text{bar}}}\left(g_{\text{bar}}\left(f\left(\frac{g_{\text{bar}}}{g_\dagger}\right) - 1\right)\right)\frac{\text{d}g_{\text{bar}}}{\text{d}r} \tag{16}$$

$$= \frac{2g_{\text{bar}}(f(\frac{g_{\text{bar}}}{g_\dagger}) - 1)}{r} + \left(f\left(\frac{g_{\text{bar}}}{g_\dagger}\right) - 1 + \frac{g_{\text{bar}}}{g_\dagger}f'\left(\frac{g_{\text{bar}}}{g_\dagger}\right)\right)\frac{\text{d}g_{\text{bar}}}{\text{d}r} \tag{17}$$

$$\therefore \rho_{\text{DM}} = \frac{g_{\text{bar}}(f(\frac{g_{\text{bar}}}{g_\dagger}) - 1)}{2\pi Gr} + \frac{1}{4\pi G}\left(f\left(\frac{g_{\text{bar}}}{g_\dagger}\right) - 1 + \frac{g_{\text{bar}}}{g_\dagger}f'\left(\frac{g_{\text{bar}}}{g_\dagger}\right)\right)\frac{\text{d}g_{\text{bar}}}{\text{d}r} \tag{18}$$

As an exemplar of the utility of equation (18), I begin by presenting the "deep MOND" limit, $f(g_{\text{bar}}/g_\dagger) = \sqrt{g_\dagger/g_{\text{bar}}}$.

$$\rho_{\text{DM}} = \frac{g_{\text{bar}}\left(\sqrt{\frac{g_\dagger}{g_{\text{bar}}}} - 1\right)}{2\pi Gr} + \frac{1}{4\pi G}\left(\sqrt{\frac{g_\dagger}{g_{\text{bar}}}} - 1 + \frac{g_{\text{bar}}}{g_\dagger}\left(-\frac{g_\dagger\sqrt{g_\dagger}}{2g_{\text{bar}}\sqrt{g_{\text{bar}}}}\right)\right)\frac{\text{d}g_{\text{bar}}}{\text{d}r} \tag{19}$$

$$= \frac{\sqrt{g_{\text{bar}}g_\dagger} - g_{\text{bar}}}{2\pi Gr} + \frac{1}{4\pi G}\left(\sqrt{\frac{g_\dagger}{g_{\text{bar}}}} - 1 - \frac{1}{2}\sqrt{\frac{g_\dagger}{g_{\text{bar}}}}\right)\frac{\text{d}g_{\text{bar}}}{\text{d}r} \tag{20}$$

$$= \frac{\sqrt{g_{\text{bar}}g_\dagger} - g_{\text{bar}}}{2\pi Gr} + \frac{1}{4\pi G}\left(\frac{1}{2}\sqrt{\frac{g_\dagger}{g_{\text{bar}}}} - 1\right)\frac{\text{d}g_{\text{bar}}}{\text{d}r} \tag{21}$$

This far out in a galaxy, the baryonic mass distribution is very close to Keplerian, $g_{\text{bar}} = \frac{GM}{r^2}$ where M = total baryonic mass. Then, $\frac{\text{d}g_{\text{bar}}}{\text{d}r} = -\frac{2GM}{r^3}$ and we get

$$\rho_{\text{DM}} = \frac{\sqrt{\frac{GM}{r^2}g_\dagger} - g_{\text{bar}}}{2\pi Gr} + \frac{1}{4\pi G}\left(\frac{1}{2}\sqrt{\frac{g_\dagger r^2}{GM}} - 1\right)\left(-\frac{2GM}{r^3}\right) \tag{22}$$

$$= \frac{1}{2\pi r^2}\sqrt{\frac{Mg_\dagger}{G}} - \frac{M}{2\pi r^3} - \frac{1}{4\pi r^2}\sqrt{\frac{Mg_\dagger}{G}} + \frac{M}{2\pi r^3} \tag{23}$$

$$= \frac{1}{4\pi r^2}\sqrt{\frac{Mg_\dagger}{G}} \tag{24}$$

I'm pleasantly surprised something as foreboding as equation (18) has such a simple limit. Furthermore, we immediately know that if dark matter exists and forms NFW or Burkert profiles then MDAR connot hold indefinitely. I've just shown that if MDAR holds strictly, then $\rho_{\text{DM}} \propto \frac{1}{r^2}$, not the $\frac{1}{r^3}$ required by the aforementioned duo.

While power laws shouldn't be deployed unnecessarily, the "deep MOND" example illustrates the utility of considering ρ_{DM}'s power law behaviour across a galaxy. Indeed we often speak of NFW as having a $\frac{1}{r}$ behaviour in the centre, $\frac{1}{r^3}$ in the outskirts and so on. The degree to which a dark matter halo is "cored" or "cuspy" can also be quantified by the best power law approximation, $\rho_{\text{DM}} \propto r^\alpha$, in a galaxy's centre. To explore $\alpha(r)$, how the best power law approximation evolves through a

galaxy, I suggest using

$$\alpha = \frac{\mathrm{d}\ln\rho_{\mathrm{DM}}}{\mathrm{d}\ln r} \tag{25}$$

$$= \frac{\mathrm{d}\ln\rho_{\mathrm{DM}}}{\mathrm{d}\rho_{\mathrm{DM}}}\frac{\mathrm{d}r}{\mathrm{d}\ln r}\frac{\mathrm{d}\rho_{\mathrm{DM}}}{\mathrm{d}r} \tag{26}$$

$$= \frac{r}{\rho_{\mathrm{DM}}}\frac{\mathrm{d}\rho_{\mathrm{DM}}}{\mathrm{d}r} \tag{27}$$

For $\frac{\mathrm{d}\rho_{\mathrm{DM}}}{\mathrm{d}r}$, differentiating equation (18) gives

$$\frac{\mathrm{d}\rho_{\mathrm{DM}}}{\mathrm{d}r} = \frac{1}{2\pi G r^2}\left[r\left\{f\left(\frac{g_{\mathrm{bar}}}{g_\dagger}\right) - 1 + \frac{g_{\mathrm{bar}}}{g_\dagger}f'\left(\frac{g_{\mathrm{bar}}}{g_\dagger}\right)\right\}\frac{\mathrm{d}g_{\mathrm{bar}}}{\mathrm{d}r} - g_{\mathrm{bar}}\left(f\left(\frac{g_{\mathrm{bar}}}{g_\dagger}\right) - 1\right)\right]$$
$$+ \frac{1}{4\pi G g_\dagger}\left(2f'\left(\frac{g_{\mathrm{bar}}}{g_\dagger}\right) + \frac{g_{\mathrm{bar}}}{g_\dagger}f''\left(\frac{g_{\mathrm{bar}}}{g_\dagger}\right)\right)\left(\frac{\mathrm{d}g_{\mathrm{bar}}}{\mathrm{d}r}\right)^2 + \frac{1}{4\pi G}\left(f\left(\frac{g_{\mathrm{bar}}}{g_\dagger}\right) - 1 + \frac{g_{\mathrm{bar}}}{g_\dagger}f'\left(\frac{g_{\mathrm{bar}}}{g_\dagger}\right)\right)\frac{\mathrm{d}^2 g_{\mathrm{bar}}}{\mathrm{d}r^2} \tag{28}$$

To apply equation (27), via equations (18) and (28), throughout a galaxy, I must assume some models for g_{bar} and $f(x)$. I intend to explore a few choices for each. Furthermore, while I suggested NFW or Burkert profiles were inconsistent with a strictly MDAR-following Universe using equation (24), we shouldn't turn off the life support yet. The "deep MOND" limit may only be a good approximation for $r \gg$ the virial radius, where the concept of "a galaxy's" dark matter halo makes little sense.

2.2   Baryonic mass distribution

My strategy is to explore popular models for ρ_{bar}. Given ρ_{bar}, I must deduce g_{bar}, $\frac{\mathrm{d}g_{\mathrm{bar}}}{\mathrm{d}r}$ and $\frac{\mathrm{d}^2 g_{\mathrm{bar}}}{\mathrm{d}r^2}$ to apply equations (27) and (28).

A favourite in the field for the baryonic mass distribution is an infinitely thin, exponential disk (Freeman 1970),

$$\Sigma_*(r) = \Sigma_0 \mathrm{e}^{-r/r_0} \tag{29}$$

where $\Sigma_*(r)$ is the surface mass density at radius, r, Σ_0 is the central surface mass density and r_0 is the scale length. In that case, Freeman (1970) finds

$$g_{\mathrm{bar}} = \frac{\pi G \Sigma_0 r}{r_0}\left(I_0(s)K_0(s) - I_1(s)K_1(s)\right) \tag{30}$$

where $s = \frac{r}{2r_0}$ and I and K are the modified Bessel functions of the first and second kind. Then, using

$$\frac{\mathrm{d}I_0(s)}{\mathrm{d}s} = I_1(s) \tag{31}$$

$$\frac{\mathrm{d}K_0(s)}{\mathrm{d}s} = -K_1(s) \tag{32}$$

$$\frac{\mathrm{d}I_n(s)}{\mathrm{d}s} = \frac{1}{2}(I_{n-1}(s) + I_{n+1}(s)) \tag{33}$$

$$\frac{\mathrm{d}K_n(s)}{\mathrm{d}s} = -\frac{1}{2}(K_{n-1}(s) + K_{n+1}(s)) \tag{34}$$

$$\frac{\mathrm{d}s}{\mathrm{d}r} = \frac{1}{2r_0} \tag{35}$$

where $n \geq 1$, we get

$$\frac{\mathrm{d}g_{\mathrm{bar}}}{\mathrm{d}r} = \frac{g_{\mathrm{bar}}}{r} + \frac{\pi G \Sigma_0 r}{2r_0^2}\left(I_1(s)K_0(s) - I_0(s)K_1(s) - \frac{1}{2}K_1(s)\left(I_0(s) + I_2(s)\right) + \frac{1}{2}I_1(s)\left(K_0(s) + K_2(s)\right)\right) \tag{36}$$

Then, a true monstrosity is

$$\frac{\mathrm{d}^2 g_{\mathrm{bar}}}{\mathrm{d}r^2} = -\frac{g_{\mathrm{bar}}}{r^2} + \frac{1}{r}\frac{\mathrm{d}g_{\mathrm{bar}}}{\mathrm{d}r} + \frac{\pi G \Sigma_0}{2r_0^2}\left(I_1(s)K_0(s) - I_0(s)K_1(s) - \frac{1}{2}K_1(s)\left(I_0(s) + I_2(s)\right) + \frac{1}{2}I_1(s)\left(K_0(s) + K_2(s)\right)\right)$$
$$+ \frac{\pi G \Sigma_0 r}{4r_0^3}\left[\frac{1}{2}\left(I_0(s) + I_2(s)\right)K_0(s) - 2I_1(s)K_1(s) + \frac{1}{2}\left(K_0(s) + K_2(s)\right)I_0(s)\right.$$
$$\left. + \frac{1}{2}\left(K_0(s) + K_2(s)\right)\left(I_0(s) + I_2(s)\right) - \frac{1}{2}K_1(s)\left(I_1(s) + \frac{1}{2}\left(I_1(s) + I_3(s)\right)\right) - \frac{1}{2}I_1(s)\left(K_1(s) + \frac{1}{2}\left(K_1(s) + K_3(s)\right)\right)\right] \tag{37}$$

While an ugly expression, I present it for completeness, so that others do not have to spend an eternity carrying out the calculation themselves and so my work may checked more easily.

Generally, the lone exponential disk is popular to describe the stellar mass distribution, but not the gaseous content (van der Kruit & Freeman 2011). While gas is thought to have a negligible impact for high and intermediate mass galaxies, one

must be more careful for low mass cases. Here, I'll be applying the "stable disk model" (see Meurer, Zheng & de Blok 2013; Zheng et al. 2013; Wong et al. 2016, and RM19 for some implementations and motivation) developed in RM19 - itself an extension to the model by Wong et al. (2016).

The model assumes the Toomre stability parameter (Toomre 1964),

$$Q = \frac{\sigma \kappa}{\pi G \Sigma} \tag{38}$$

is constant throughout the galaxy. In equation (38), σ is the disk's particles' velocity dispersion, Σ is its surface mass density and κ is the epicycle frequency defined as

$$\kappa(r) = \frac{V(r)}{r} \sqrt{2 \left(1 + \frac{r}{V(r)} \frac{dV(r)}{dr} \right)} \tag{39}$$

where $V(r)$ is the rotation speed at a radius, r. Equation (38) can be extended to account for a galaxy made from stellar and gaseous disks - the preferred approach in practice. RM19's stable disk model is also an advancement on thin exponential disk as it accounts for the three dimensional distribution of stars and gas - something I found to have non-trivial consequence when developing the model's code.

I am not aware of any analytic methods to determine g_{bar} or its derivatives for the stable disk model. Therefore, I'll calculate g_{bar} using the numerical integration described in RM19 - particularly making use of equation 64 in that work. $\frac{dg_{\text{bar}}}{dr}$ and $\frac{d^2 g_{\text{bar}}}{dr^2}$ cannot be simply evaluated by $\frac{dy}{dx} \approx \frac{\delta y}{\delta x}$ because there would be too many small scale fluctuations skewing the result. Instead, I interpolated g_{bar} using a quintic spline and used its derivatives. By blind experimentation, I found choosing every 35th data point as a knot, corresponding to intervals of $\frac{7}{10} r_0$, gave the smoothest spline derivatives. Unfortunately, I couldn't remove all unwanted oscillations - indeed, with only a fifth order spline, Runge's phenomenon makes the task impossible. Hence, I'm only going to consider the inner 75% of the radial range, where the results are more reliable[3]. This is not actually as bad a problem as it sounds. RM19's stable disk implementation relies on extending the disk beyond the truncation radius, R_{max}, so the disk doesn't end abruptly and $g_{\text{bar}} \nrightarrow \infty$ as $r \to R_{\text{max}}$. Furthermore, extending the disk is physically sensible; it doesn't make sense for disks to abruptly and totally end at a radius, R_{max}, when $\rho_{\text{bar}}(r) \nrightarrow 0$ as $r \to R_{\text{max}}$. Removing the outer 25% of the radial range usually only removes this disk extension.

It would be remiss of me not to mention there are other models for the gaseous distribution. For example, Karukes & Salucci (2016) had moderate success modelling the rotation curves of dwarf disk galaxies using Tonini et al. (2006)'s model where the gas forms an exponential disk with thrice the scale length of the stellar disk. I didn't implement their model because there would be too many free parameters to vary. Overall, there isn't a consensus in the literature on how to model gas.

Both the exponential and stable disks ignore the bulge, which is thought to follow a Sersic profile. While I developed some code to model a Sersic component[4] to a galaxy, I'm not going to include that here. Primarily it's so that I don't complicate the issue - the number of combinations of interpolating function and baryonic mass distribution grows very quickly. However, it's also worth noting only a fifth of MLS16's sample galaxies had a bulge. Hence their observation of MDAR stands primarily on observing bulgeless galaxies.

As an aside, it's worth pointing out no matter what baryonic mass distribution I choose, it will automatically follow the Baryonic Tully Fischer Relation (BTFR). The BTFR follows directly from MDAR; the following argument shows it need not be added in "by hand."

As $r \to \infty$, we can simply use the deep-MOND dark matter density limit, equation (24), to model the complete dark matter distribution. Hence,

$$M_{\text{DM}}(r) = \int_0^r 4\pi r^2 \rho_{\text{DM}} \, dr \tag{40}$$

$$= \int_0^r 4\pi r^2 \left(\frac{1}{4\pi r^2} \sqrt{\frac{M_{\text{bar}} g_\dagger}{G}} \right) dr \tag{41}$$

$$= r \sqrt{\frac{M_{\text{bar}} g_\dagger}{G}} \tag{42}$$

As explained earlier, this far out in a galaxy, the baryonic mass distribution is essentially a point mass, M_{bar}, and since the

---

[3] The complete code used in RM19 and the present paper is available at https://github.com/VirinchiRallabhandi/GalaxyModels. In particular, the implementation I'm applying here is "GalaxyModel14.java" for the majority of the calculations and "dark matter slopes.py" for the graphs and interpolation

[4] Available at the same location provided in the footnote directly above

ρ_{DM} is spherically symmetric, the only gravitational forces relevant at a radius, r, are those at a lower radius. Thus,

$$\lim_{r \to \infty} V(r) = \lim_{r \to \infty} \sqrt{\frac{GM_{\text{total}}}{r}} \tag{43}$$

$$= \lim_{r \to \infty} \sqrt{\frac{G}{r}\left(M_{\text{bar}} + r\sqrt{\frac{M_{\text{bar}}g_\dagger}{G}}\right)} \tag{44}$$

$$= \lim_{r \to \infty} \sqrt{\frac{GM_{\text{bar}}}{r} + \sqrt{GM_{\text{bar}}g_\dagger}} \tag{45}$$

$$= (GM_{\text{bar}}g_\dagger)^{1/4} \tag{46}$$

Then, taking $\lim_{r \to \infty} V(r) = V_f$, the rotation velocity on the flat part of the rotation curve,

$$M_{\text{bar}} = \frac{1}{Gg_\dagger}V_f^4 \tag{47}$$

which is indeed the archetypal BTFR, $M_{\text{bar}} \propto V_f^4$ with MOND predicting a proportionality constant, $\frac{1}{Gg_\dagger}$.

2.3 MOND interpolating functions

While the equations thus far apply for arbitrary interpolating functions, f, I have to choose a specific functional form for calculations. For each f, I require f' and f'' to use equation (28). The most natural choice is

$$f_1(x) = \frac{1}{1 - e^{-\sqrt{x}}} \tag{48}$$

because MLS16 chose it as the function they believed best fit their data. However, Milgrom (2016) showed

$$f_2(x) = \frac{1 + \sqrt{1 + \frac{4}{x}}}{2} \tag{49}$$

and

$$f_3(x) = \tanh^{-a}(x^{1/2a}) \tag{50}$$

also fit the data very well; for f_3 Milgrom (2016) suggests $a = 1.75$. For the 1st and 2nd derivatives, we get

$$f_1'(x) = -\frac{(-e^{-\sqrt{x}})(-\frac{1}{2\sqrt{x}})}{(1 - e^{-\sqrt{x}})^2} \tag{51}$$

$$= -\frac{e^{-\sqrt{x}}}{2\sqrt{x}(1 - e^{-\sqrt{x}})^2} \tag{52}$$

$$\therefore f_1''(x) = -\frac{1}{2x(1 - e^{-\sqrt{x}})^4}\left\{-\frac{1}{2\sqrt{x}}e^{-\sqrt{x}}(\sqrt{x}(1 - e^{-\sqrt{x}})^2) - e^{-\sqrt{x}}\left(\frac{1}{2\sqrt{x}}(1 - e^{-\sqrt{x}})^2 + 2\sqrt{x}(1 - e^{-\sqrt{x}})(\frac{1}{2\sqrt{x}}e^{-\sqrt{x}})\right)\right\} \tag{53}$$

$$= \frac{1}{4x(1 - e^{-\sqrt{x}})^4}\left\{e^{-\sqrt{x}}(1 - e^{-\sqrt{x}})^2 + e^{-\sqrt{x}}\left(\frac{1}{\sqrt{x}}(1 - e^{-\sqrt{x}})^2 + 2(1 - e^{-\sqrt{x}})e^{-\sqrt{x}}\right)\right\} \tag{54}$$

$$= \frac{e^{-\sqrt{x}}(1 - e^{-\sqrt{x}}) + e^{-\sqrt{x}}\left(\frac{1}{\sqrt{x}}(1 - e^{-\sqrt{x}}) + 2e^{-\sqrt{x}}\right)}{4x(1 - e^{-\sqrt{x}})^3} \tag{55}$$

$$= \frac{e^{-\sqrt{x}}(1 - e^{-\sqrt{x}})\left(1 + \frac{1}{\sqrt{x}}\right) + 2e^{-2\sqrt{x}}}{4x(1 - e^{-\sqrt{x}})^3} \tag{56}$$

for f_1,

$$f_2'(x) = \frac{-4/x^2}{4\sqrt{1 + \frac{4}{x}}} \tag{57}$$

$$= -\frac{1}{x^2\sqrt{1 + \frac{4}{x}}} \tag{58}$$

$$\therefore f_2''(x) = \frac{2x\sqrt{1 + \frac{4}{x}} + x^2\left(\frac{1}{2\sqrt{1+4/x}}\left(-\frac{4}{x^2}\right)\right)}{x^4\left(1 + \frac{4}{x}\right)} \tag{59}$$

$$= \frac{2x\sqrt{1 + \frac{4}{x}} - \frac{2}{\sqrt{1+4/x}}}{x^4\left(1 + \frac{4}{x}\right)} \tag{60}$$

$$= \frac{2x\left(1 + \frac{4}{x}\right) - 2}{x^4\left(1 + \frac{4}{x}\right)^{3/2}} \tag{61}$$

$$= \frac{2(x + 3)}{x^4\left(1 + \frac{4}{x}\right)^{3/2}} \tag{62}$$

for f_2 and

$$f_3'(x) = (-a\tanh^{-(a+1)}(x^{1/2a}))(\text{sech}^2(x^{1/2a}))\left(\frac{x^{1/2a-1}}{2a}\right) \tag{63}$$

$$= -\frac{1}{2}x^{1/2a-1}\tanh^{-(a+1)}(x^{1/2a})\,\text{sech}^2(x^{1/2a}) \tag{64}$$

$$\therefore f_3''(x) = \left(\frac{1}{2} - \frac{1}{4a}\right)x^{1/2a-2}\tanh^{-(a+1)}(x^{1/2a})\,\text{sech}^2(x^{1/2a}) + \frac{a+1}{4a}x^{1/a-2}\tanh^{-(a+2)}(x^{1/2a})\,\text{sech}^4(x^{1/2a})$$

$$+ \frac{1}{2a}x^{1/a-2}\tanh^{-a}(x^{1/2a})\,\text{sech}^2(x^{1/2a}) \tag{65}$$

for f_3. Intuitively, I don't expect the behaviour of these three functions to give radically different results because they are all very similar across the acceleration range studied by MLS16. However, I'm still going to test them all for completeness.

3   RESULTS

After all that maths, there isn't really much left to do. My plan is to try many different realistic calibrations for the baryonic mass distribution with each MOND interpolating function. For each, I'll calculate $\frac{d\ln\rho_{\text{DM}}}{d\ln r}$ - to compare it against what's expected for popular dark matter halo profiles like NFW. Because of equation (24), I already know my calculated value will be -2 in the limit. However, if that limit is at radii on the order of the virial radius, then the limit is rather useless because a galaxy is unlikely to be rotationally supported that far out. Throughout this section, I'm taking $g_\dagger = 1.2 \times 10^{-10}$, the same value as MLS16, and $a = 1.75$ for f_3, the value suggested by Milgrom (2016).

First up, the exponential disk, $\Sigma_* = \Sigma_0 e^{-r/r_0}$. I need to choose realistic values for Σ_0 and r_0. Choosing Σ_0 is the same as choosing the stellar mass given r_0 because

$$M_* = \int_0^\infty 2\pi r\Sigma_0 e^{-r/r_0}\,dr \tag{66}$$

$$= 2\pi\Sigma_0 r_0^2 \tag{67}$$

$$\therefore \Sigma_0 = \frac{M_*}{2\pi r_0^2} \tag{68}$$

In RM19, we showed one could find a scaling between r_0 and M_* with some intermediate parameters. However, all these scaling relations have non-negligible scatter. Therefore, as in section 6 of RM19, I'm not going to impose a strict relation between r_0 and M_*. Rather, I'll try a range of combinations for each. Through the literature review in RM19, we found the range of galaxy masses and r_0 is at most between $10^{39} - 10^{42}$ kg and $10^{19} - 2 \times 10^{20}$ m respectively. Taking 25 model galaxies across this range as representatives, I get figures $1 - 3$ by going through the interpolating functions. Contrary to my expectations, changing the interpolating function has quite an appreciable impact. f_2 tends to have a greater global minimum than the rest and f_3 tends to rise most slowly from the global minimum. As an by-product, $\frac{d\ln\rho_{\text{DM}}}{d\ln r}$ occasionally doesn't get close to it's -2 asymptote even at $r = 20r_0$, where I've cut-off the graphs.
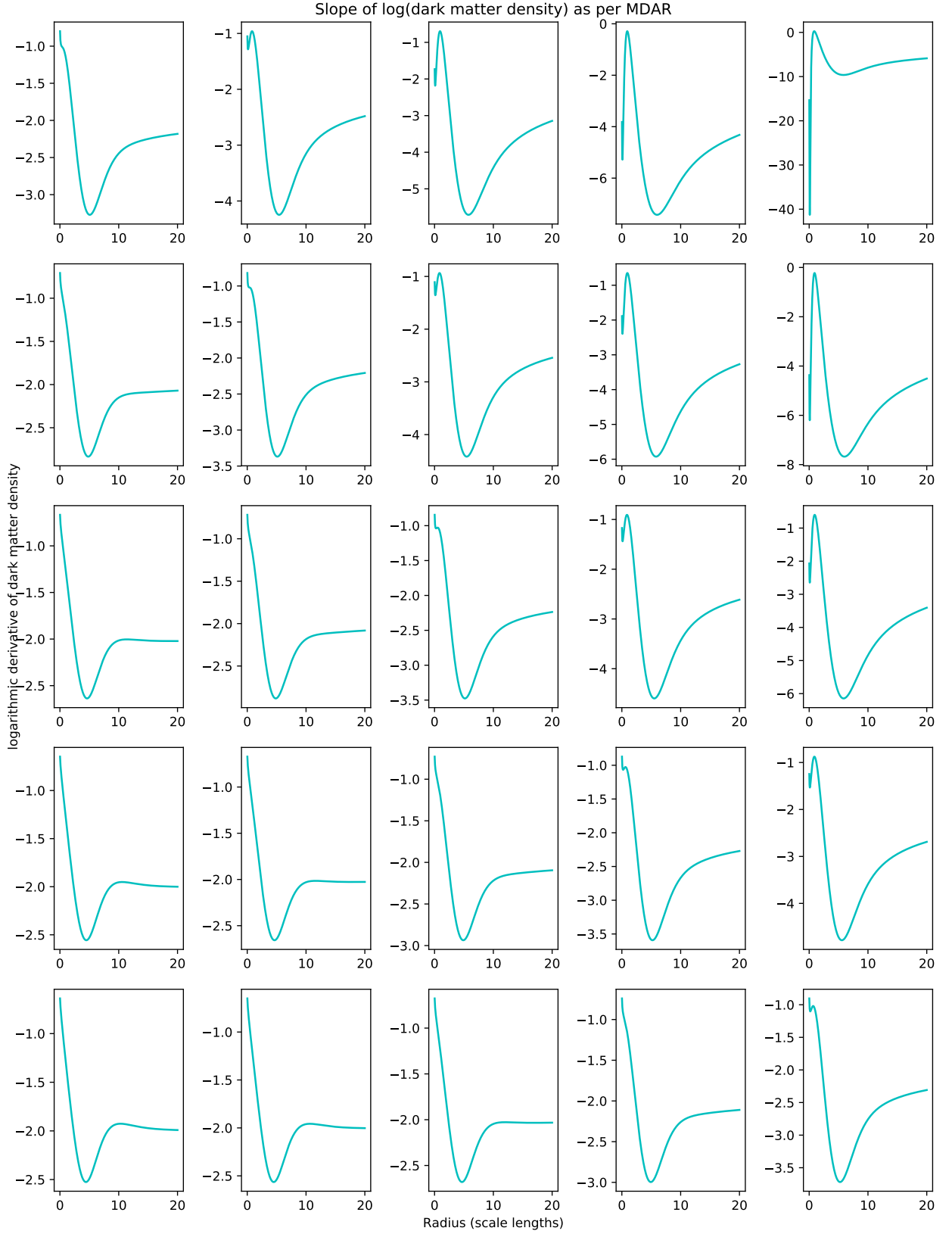
Slope of log(dark matter density) as per MDAR
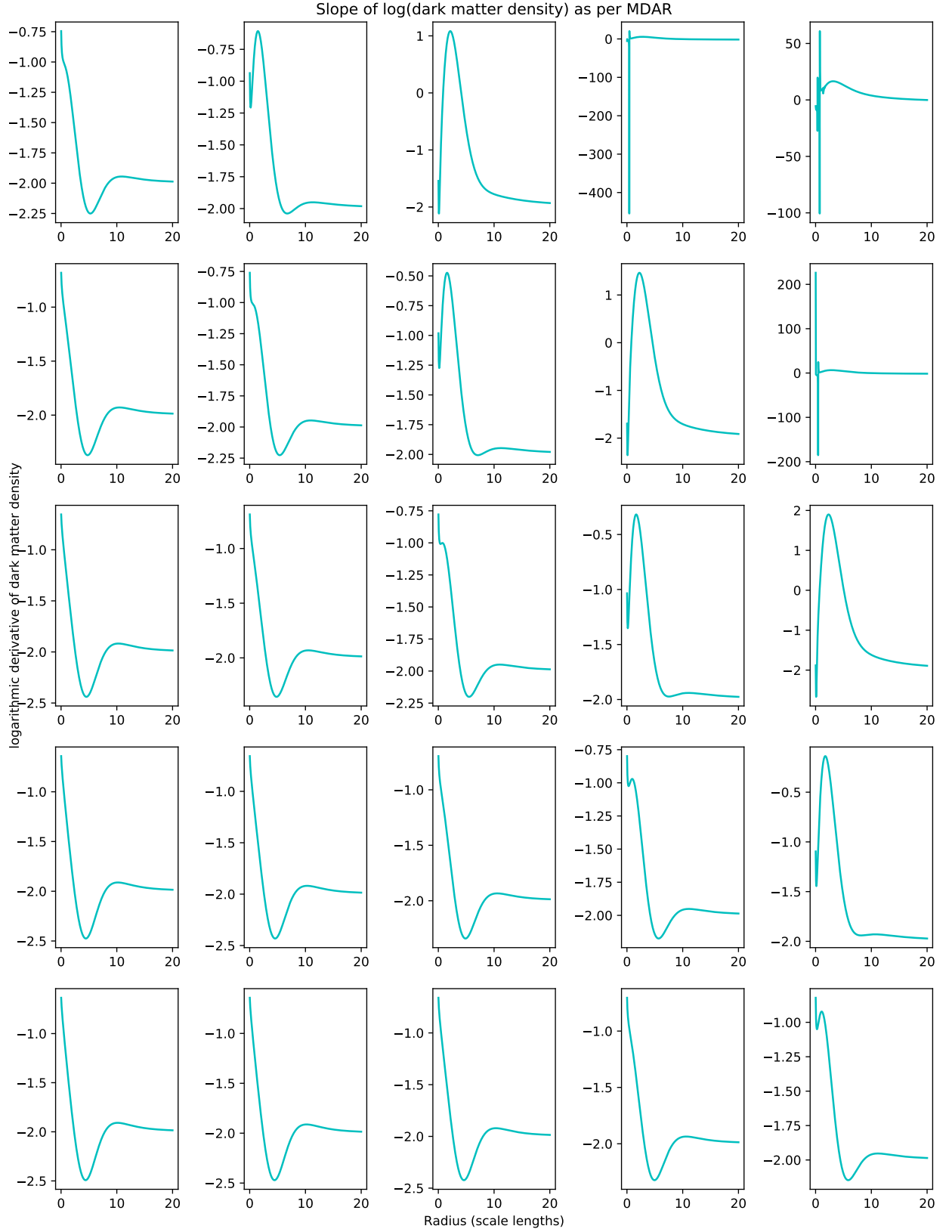
Figure 1. Cell (i, j) - indexing with $(0, 0)$ in the top left, i being the row index and j being the column index - gives $\frac{\mathrm{d}\ln\rho_{DM}}{\mathrm{d}\ln r}$ as a function of r - in units of r_0 - for a galaxy with $r_0 = 10^{19} \times 20^{i/4}$ m and $M_* = 10^{39} \times 1000^{j/4}$ kg using f_1 as the interpolating function.
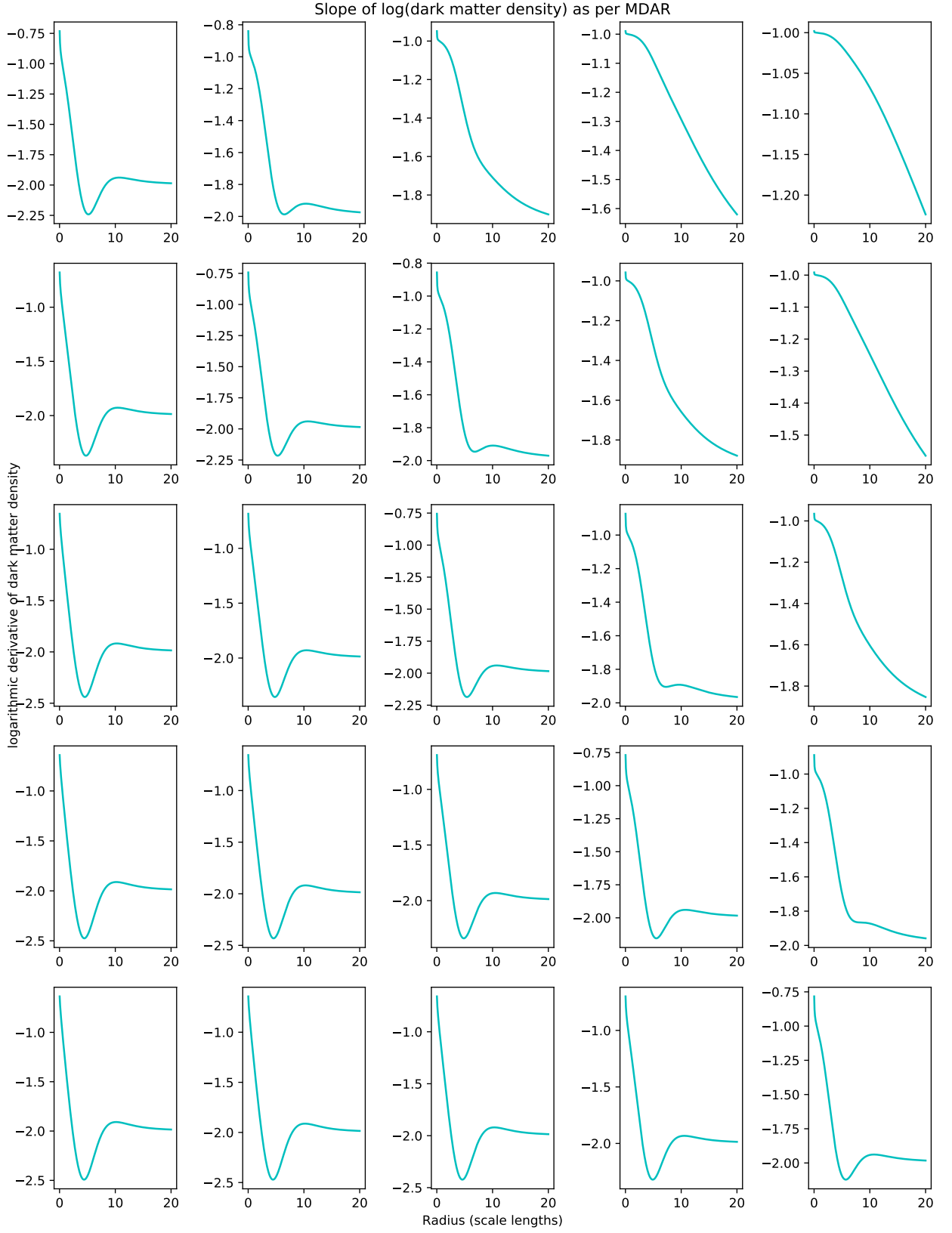
Figure 2. Cell (i, j) - indexing with $(0, 0)$ in the top left, i being the row index and j being the column index - gives $\frac{\mathrm{d}\ln\rho_{DM}}{\mathrm{d}\ln r}$ as a function of r - in units of r_0 - for a galaxy with $r_0 = 10^{19} \times 20^{i/4}$ m and $M_* = 10^{39} \times 1000^{j/4}$ kg using f_2 as the interpolating function.

Figure 3. Cell (i, j) - indexing with $(0, 0)$ in the top left, i being the row index and j being the column index - gives $\frac{d\ln\rho_{DM}}{d\ln r}$ as a function of r - in units of r_0 - for a galaxy with $r_0 = 10^{19} \times 20^{i/4}$ m and $M_* = 10^{39} \times 1000^{j/4}$ kg using f_3 as the interpolating function.

All the popular dark matter halo profiles I namechecked earlier - NFW, Burkert, isothermal sphere, cored isothermal sphere and DC14 - have monotonically decreasing $\frac{d\ln\rho_{DM}}{d\ln r}$ profiles. Only very few of my model galaxies - a representative sample of the various possible combinations of r_0 and Σ_0 in real galaxies - actually have monotonically decreasing $\frac{d\ln\rho_{DM}}{d\ln r}$. The ones that do are very high mass, low scale length galaxies - an unlikely combination (Wong et al. 2016) - with interpolating function, f_2. Using f_1, again there are a few problems with very high mass, low scale length galaxies. However, overall, it's clear the $\frac{d\ln\rho_{DM}}{d\ln r}$ profiles start between -1 and -0.5 - a cusp rather than a core - and then dip down to about -2.5 at $r \approx 5r_0$ and rise back up to -2 at $r \approx 10r_0$. However, I don't know if such a dip and rise can be detected within the baryonic extent of galactic disks. For example, Meurer et al. (2018) found $R_{max} = (4.7 \pm 0.8)r_0$ where R_{max} is the disk's truncation radius. $4.7r_0$ is too small to distinguish my profiles in figures $1 - 3$ from NFW, Burkert, etc. Yet, Ianjamasimanana et al. (2015) were plotting HI velocity dispersion all the way out to about 15 scale lengths in some galaxies; that's more than enough to observe the dip and rise in $\frac{d\ln\rho_{DM}}{d\ln r}$ in figures $1 - 3$. I'll leave it to the observers to squabble over the discrepancy.

Figures $1 - 3$ give a broad description of the implied dark matter density profiles. However, I've ignored all possible calibration between M_* and r_0 in producing these figures. We see non-trivial variations in $\frac{d\ln\rho_{DM}}{d\ln r}$ across each figure. To better understand these variations, I want to explore $\frac{d\ln\rho_{DM}}{d\ln r}$ within model galaxies which abide by observed scaling relations - a task for which RM19's stable disk model is well suited.

RM19's stable disk model is built upon one independent variable, V_{final}, the rotation speed at the disk's edge. From there, the rotation curve is deduced by the Universal Rotation Curve (URC) (Persic & Salucci 1991; Persic, Salucci & Stel 1996) and the stellar and gaseous mass distributions by various scaling relations and the constant Q property. The dark matter distribution was assumed to be a free parameter which adjusts so that the URC is reproduced given the deduced baryonic mass distribution. However, that doesn't guarantee strict adherence to MDAR. The rotation curve is intrinsically linked to MDAR because

$$\frac{V(r)^2}{r} = g_{obs} = g_{bar} f(g_{bar}/g_\dagger) \tag{69}$$

Hence, $V(r)$ is calculated from g_{bar} when one assumes MDAR holds strictly. But I need to know $V(r)$ to apply the stable disk model because the epicycle frequency is a function of $V(r)$.

The only solution I see is to iteratively improve $V(r)$, ρ_* and ρ_g - the rotation curve and stellar & gaseous volume mass density - so that we get both constant Q and strict MDAR. Using my favourite problem solving strategy, guess and check, I found five iterations suffices for $V(r)$, ρ_* and ρ_g to converge close to an equilibrium. The resulting $\frac{d\ln\rho_{DM}}{d\ln r}$ profiles are shown in figure 4. As explained earlier, I've only graphed the inner 75% of the radial range. The scale lengths referenced in the figure are the initial (before iteration) r_0 values for the exponential stellar disk embedded within the disk. The profiles are somewhat different to the pure exponential disks. The profiles are still rarely monotonic, but I believe that might only be because Runge's phenomenon is affecting the results. Such concerns may be alleviated by using far greater computing power in evaluating g_{bar}. I would have liked to apply the stable disk model for $V_{final} < 125$ km/s[5], but alas, the iteration between initially assumed rotation curve and strict MDAR rotation curve doesn't converge. In fact, it's very difficult to rigorously prove convergence in any case. For example, the harmonic series' partial sums don't intuitively look like they diverge, but they do anyway.

However, one may still glean useful information form figure 4. Like the thin exponential disk case, $\frac{d\ln\rho_{DM}}{d\ln r}$ dips much further below -2 when using f_3 compared to f_1 or f_2. In fact, when applying f_1 and f_2, $\frac{d\ln\rho_{DM}}{d\ln r}$ doesn't always dip below -2. This is a marked difference to the thin exponential disk case and illustrates that gas is a non-trivial player in rotation curve and dark matter studies. In the cases where $\frac{d\ln\rho_{DM}}{d\ln r}$ dips below -2, it doesn't often make it back up to -2 within the radial range plotted. Yet, from equation (24), we know all the subplots must asymptote to -2. Therefore, adding gas - much more influential in galaxies' outer parts - has pushed the global minimum in $\frac{d\ln\rho_{DM}}{d\ln r}$ further out compared to the thin exponential disks considered earlier. In all 18 cases, $-1 \lesssim \frac{d\ln\rho_{DM}}{d\ln r}\big|_{r=0} \lesssim -0.5$, quite a cuspy centre[6]. None of the established dark matter density profiles can reproduce the profiles in figure 4, but in some cases they are qualitatively alike. DC14 seems the best to me - perhaps an unsurprising result as it's the only one taking into account baryonic processes such as the gas distribution so central to distinguishing figure 4 from figures $1 - 3$.

4   CONCLUSION

Inspired by MLS16's result, I set out to explore what it takes to strictly reproduce MDAR - the quintessential MOND law - within the dark matter paradigm. I've assumed dark matter is massive, interacts solely gravitationally with all other

---

[5] By this I mean V_{final} was originally set to 125 km/s; the iteration process will usually change V_{final} and other parameters, such as r_0.

[6] It's not actually possible to find $\frac{d\ln\rho_{DM}}{d\ln r}$ directly from equation (27) because of dividing by zero issues in equation (28). I'm taking $\frac{d\ln\rho_{DM}}{d\ln r}\big|_{r=0}$ as $\frac{d\ln\rho_{DM}}{d\ln r}$ at the innermost r value it's calculated - namely $r = 0.02r_0$.
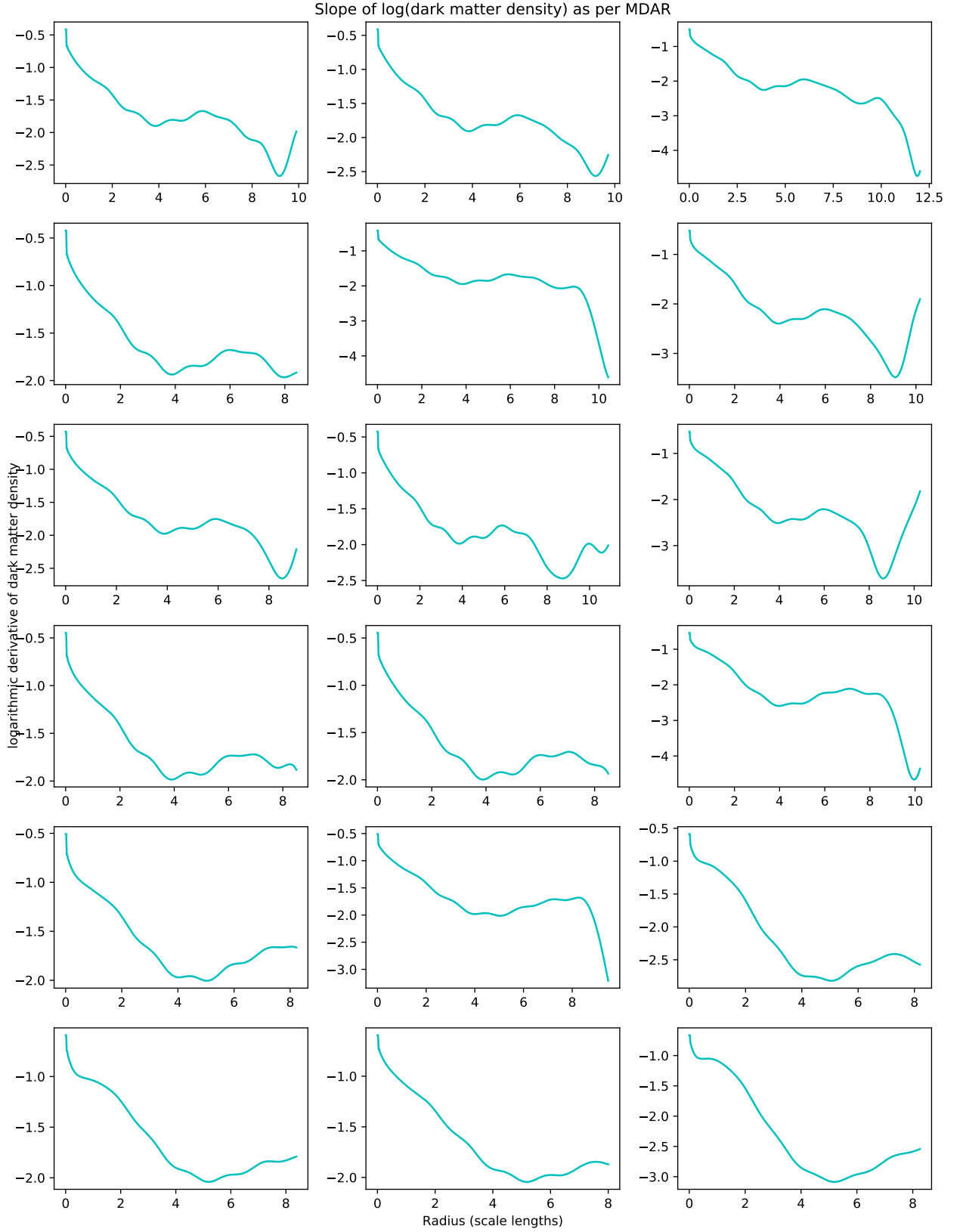
Figure 4. Cell (i, j) - indexing with $(0, 0)$ in the top left, i being the row index and j being the column index - gives the $\frac{d \ln \rho_{DM}}{d \ln r}$ profile for the stable disk model initialised with $V_{final} = (125 + 25i)$ km/s and using interpolating function, f_{j+1}.

massive particles, moves at non-relativistic speeds and is distributed in a spherically symmetric manner. Given a baryonic mass distribution and the assumption MDAR holds strictly, I was able determine various properties of the dark matter using Poisson's law. These included its volume mass density as a function of radius, equation (18), its distribution as $r \to \infty$, equation (24), and the exponent of its best power law approximation, equation (27) for $\frac{\mathrm{d}\ln\rho_{\mathrm{DM}}}{\mathrm{d}\ln r}$. A further consequence of assuming strict MDAR is the BTFR, equation (47), must hold. All of these results apply generally.

However, to make them concrete, I tried various commonly applied prescriptions for MOND interpolating function consistent with MLS16's result and baryonic mass distribution. I found there are significant differences between all the cases. I found the $r \to \infty$ limit was inconsistent with most established dark matter density profiles, except the cored and normal isothermal spheres. However, getting close to the limit is difficult within galaxies' observable radial range. Instead, to better assess how well the strict MDAR dark matter profiles correlated with the established profiles from simulations, I decided to track $\frac{\mathrm{d}\ln\rho_{\mathrm{DM}}}{\mathrm{d}\ln r}$ through a galaxy. I found $\frac{\mathrm{d}\ln\rho_{\mathrm{DM}}}{\mathrm{d}\ln r}$ is rarely monotonically decreasing as in the expected profiles from ΛCDM simulations. The disparity is greatest when considering a thin exponential disk and interpolating function, f_3, but somewhat smaller for the other two interpolating functions tried and the stable disk model - a well calibrated method to derive the 3D distribution of stars and gas within a galaxy.

My hope is analysis such as these will contribute to disproving either the MOND or dark matter paradigms. In MOND, MDAR must hold strictly. If MDAR holds strictly as MLS16 suggest, then there are major problems for ΛCDM because dark matter profiles predicted by simulations disagree with the ones I've shown are required for strict MDAR. As I mentioned earlier, MDAR has qualitatively been reproduced by many scientists (Navarro et al. 2017; Ludlow et al. 2017; Keller & Wadsley 2017, are the examples I cited earlier) under ΛCDM. Therefore, to truly settle the debate, MLS16 need to be more forthright about how strictly MDAR holds within each galaxy[7]. If MDAR holds strictly, ΛCDM is reeling; if MDAR doesn't hold strictly, then the central tenet of MOND is disproven. The issue of MDAR holding strictly is further complicated because there are many different interpolating functions to check. I've shown that although many disparate functions are consistent with MLS16's data, they have significantly different implications for dynamics within a galaxy.

While it's very easy to fall deep into this bottomless well of debate between MOND and dark matter, one should remember it's possible ΛCDM and MOND are both barking up the wrong tree. For example, we've now seen galaxies with surprisingly little dark matter (van Dokkum et al. 2018, 2019). If the results are correct - as they seem to be - then the strict MDAR mass modelling presented here is for nought. Similarly, ΛCDM supporters would have to rethink the theory of galaxies forming within dark matter halos.

It is of course surprises such as these which keep us in the field. I don't claim to have settled the debate between MOND and ΛCDM. But I do claim to present a result regarding some specific subtleties at the boundary between the two theories. As with all great mysteries, the resolution is elusive and each question on the path seems to throw up more follow-up questions than answers.

REFERENCES

Burkert A., 1995, ApJ Letters, 447, L25
Di Cintio A., Brook C. B., Maccio A. V., Stinson G. S., Knebe A., Dutton A. A., Wadsley J., 2014, MNRAS, 437, 415
Freeman K. C., 1970, ApJ, 160, 811
Gentile G., Famaey B., de Blok W. J. G., 2011, A&A, 527, A76
Ianjamasimanana R., de Blok W. J. G., Walter F., Heald G. H., Caldu-Primo A., Jarrett T. H., 2015, AJ, 150, 47
Karukes E. V, Salucci P., 2016, MNRAS, 465, 4703
Keller B. W., Wadsley J. W., 2017, ApJ Letters, 835, L17
Ludlow A. D. et al., 2017, Phys. Rev. Lett., 118, 161103
McGaugh S. S., Lelli F., Schombert J. M., 2016, Phys. Rev. Lett., 117, 201101 (MLS16)
Meurer G. R., Zheng Z., de Blok W. J. G., 2013, MNRAS, 429, 2537
Meurer G. R., Obreschkow D., Wong O. I., Zheng Z., Audcent-Ross F. M., Hanish D. J., 2018, MNRAS, 476, 1624
Milgrom M., 2016, preprint (arXiv:1609.06642)
Navarro J. F., Frenk C. S., White S. D., 1997, ApJ, 490, 493
Navarro J. F., Benitez-Llambay A., Fattahi A., Frenk C. S., Ludlow A. D., Oman K. A., Schaller M., Theuns T., 2017, MNRAS, 471, 1841

---

[7] I accept it may not be possible to do this within observational uncertainties imposed by current technology

Persic M., Salucci P., 1991, ApJ, 368, 60

Persic M., Salucci P., Stel F., 1996, MNRAS, 281, 27

Rallabhandi V., Meurer G., 2019, Internship report, International Centre for Radio Astronomy Research, available at https://github.com/VirinchiRallabhandi/GalaxyModels (RM19)

Sanders R. H., 1990, A&AR, 2, 1

Tonini C., Lapi A., Shankar F., Salucci P., 2006, ApJ, 638, L13

Toomre A, 1964, ApJ, 139, 1217

van der Kruit P. C, Freeman K. C., 2011, ARAA, 49, 301

van Dokkum P. et al., 2018, Nature, 555, 629

van Dokkum P., Danieli S., Abraham R., Conroy C., Romanowsky A. J., 2019, ApJ Letters, 874, 8

Wong O. I., Meurer G. R., Zheng Z., Heckman T. M., Thilker D. A., Zwaan M. A., 2016, MNRAS, 460, 1106

Zheng Z., Meurer G. R., Heckman T. M., Thilker D. A., Zwaan M. A., 2013, MNRAS, 434, 3389

This paper has been typeset from a TEX/LATEX file prepared by the author.